Hybrids made of a Fe-containing Wells-Dawson polyoxometalate and carbon nanomaterials as promising electrocatalysts for the oxygen reduction reaction

Hugo C. Novais[a], Bruno Jarrais[a], Israël-Martyr Mbomekallé[b], Anne-Lucie Teillout[b], Pedro de Oliveira[b], Cristina Freire[a], Diana M. Fernandes[a*]

[a] REQUIMTE/Departamento de Química e Bioquímica, Faculdade de Ciências, Universidade do Porto, 4169-007 Porto, Portugal.

[b] Equipe d'Electrochimie et de Photo-électrochimie, Institut de Chimie Physique, UMR 8000 CNRS, Faculté des Sciences d'Orsay, Université Paris-Saclay, , Orsay F-91405, France.

*Corresponding authors: Dr. Diana M. Fernandes (diana.fernandes@fc.up.pt)

Keywords: Oxygen Reduction Reaction, Electrocatalysis, Carbon Materials, Polyoxometalate

S1. Experimental

S1.1. Materials and solvents

The POM salt $K_7[P_2W_{17}(FeOH_2)O_{61}] \cdot 20H_2O$ was prepared according to the reported procedure.[1]

Potassium hydroxide (> 99%, Sigma-Aldrich), Nafion® at 5 wt.% (lower aliphatic alcohols and water, Sigma-Aldrich), isopropanol (99.5 %, Sigma-Aldrich), sulfuric acid (95–97 %, Merck), platinum 20 % on carbon black (Pt/C, HiSPEC® 3000, Alfa Aesar) were used as received from the suppliers. Commercial graphene (sample denoted as GF) was from Graphene Technologies (Lot #GTX-7/6-10.4.13). Multi-walled carbon nanotubes (sample denoted as MWCNT) were commercially obtained from Nanocyl S.A., Ref. 3100 MWCNT (>95% carbon purity; 9.5 nm average diameter). For electrolyte and composites preparation, ultrapure water (18.2 MΩ cm at 25ºC, Interlab) was always used.

S1.2. Physicochemical characterization

A Jasco FT/IR-460 Plus spectrophotometer was used to acquire the Fourier-transformed infrared (FTIR) spectra (64 scans, resolution of 4 cm^{-1}, between 400 and 4000 cm^{-1}). The spectra were obtained for samples dispersed (0.2 wt. %) in KBr pellets (spectroscopic grade, Merck).

X-ray photoelectron spectroscopy (XPS) measurements were performed at "Centro de Materiais da Universidade do Porto" (CEMUP), Portugal, in a VG Scientific ESCALAB 200A spectrometer with non-monochromatized Al Kα radiation (1486.6 eV). Potential deviations induced by electric charge of the samples were corrected using the C 1s band at 284.6 eV as an internal standard. The high-resolution spectra analysis and deconvolution was performed with the CasaXPS software.

The scanning electron microscopy/energy-dispersive X-ray spectroscopy (SEM/EDX) images were acquired using a high resolution (Schottky) environmental SEM with X-ray

microanalysis and electron backscattered diffraction analysis (Quanta 400 FEG ESEM/EDAX Genesis X4M), in high-vacuum conditions, at CEMUP.

S1.3. ORR electrochemical tests

An Autolab PGSTAT 302N (EcoChimie B.V.) potentiostat/galvanostat, controlled by the NOVA v2.1 software was employed for the cyclic voltammetry (CV) and linear sweep voltammetry (LSV) studies. The experiments were carried out at room temperature using a conventional three-electrode compartment cell.

A modified glassy carbon rotating disk electrode, RDE (Metrohm, 3 mm diameter) was used as the working electrode while an Ag/AgCl (Metrohm, 3 M KCl) and a carbon rod (Metrohm, 2 mm diameter) were used as reference and counter electrodes, respectively. Prior to modification of the bare electrodes, the RDE was polished with 6, 3 and 1 μM diamond polishing pastes (Buehler) on a MicroCloth polishing pad (BAS), followed by washing with ultrapure water. Then, a 2×2.5 μL drop of selected electrocatalyst dispersion was deposited on the RDE and left to dry under an airflow.

For the RDE modification, 1 mg of EC ($P_2W_{17}Fe@CM$ or Pt/C) and a mixture of 125 μL of isopropanol, 125 μL of ultrapure water and 20 μL of Nafion (5 wt%) were ultrasonically dispersed for 20 min. The electrochemical tests were carried out in N_2- or O_2-saturated KOH (0.1 mol dm^{-3}). To achieve this, the electrolyte was bubbled for 40 min with the selected gas.

The CV measurements were performed at 0.005 V s^{-1} and the LSV ones at 0.005 V s^{-1} with rotation speeds in the range 400 - 3000 rpm. The ORR current obtained in N_2-saturated KOH (0.1 mol dm^{-3}) was subtracted from that obtained in O_2-saturated KOH. The chronoamperometry (CA) tests were done at a potential (E) of 0.5 V vs. RHE and a rotation speed of 1600 rpm for 36000 s. Resistance to methanol was evaluated by CA at $E = 0.5$ V vs. RHE and 1600 rpm for 2500 s.

The onset potential (E_{onset}) is defined as the potential at which the reduction of O_2 begins and it was determined as described in the literature. [2] The electrochemical potentials and the E_{onset} values determined vs. Ag/AgCl were converted to the reversible hydrogen electrode (RHE) using the following equation:

$$E_{(RHE)} = E_{(Ag/AgCl)} + 0.059 \text{ pH} + E^o_{(Ag/AgCl)} \quad (S1)$$

where $E_{(RHE)}$ is the potential vs. RHE, $E^o_{(Ag/AgCl)} = 0.1976$ V (25 °C) and $E_{(Ag/AgCl)}$ is the potential measured vs. Ag/AgCl.[3]

To analyse the LSV data and the number of electrons transferred per O_2 molecule (n_{O2}) in the oxygen reduction reaction the Koutecky-Levich (K-L) equation was used:

$$\frac{1}{j} = \frac{1}{j_L} + \frac{1}{j_k} = \frac{1}{B\omega^{1/2}} + \frac{1}{j_k} \quad (S2)$$

Here, j is the current density measured, j_L the diffusion-limiting current density, j_k the kinetic current density and ω the angular velocity. The parameter B is associated to the diffusion limiting current density expressed by the following equation:

$$B = 0.2 \, n_{O2}F \, (D_{O2})^{2/3} v^{-1/6} C_{O2} \quad (S3)$$

with $F = 96\,485$ C mol^{-1}, D_{O2} the O_2 diffusion coefficient, v the electrolyte kinematic viscosity and C_{O2} the O_2 bulk concentration. For rotation speeds in rpm is adopted a constant 0.2. Additionally, in the electrolyte used KOH (0.1 mol dm^{-3}): $D_{O2} = 1.95 \times 10^{-5}$ cm^2 s^{-1}, $v = 0.008977$ cm^2 s^{-1} and $C_{O2} = 1.15 \times 10^{-3}$ mol dm^{-3}. [4]

Tafel plots ($E_{(RHE)}$ vs. log j_k) were obtained after the measured LSV currents were rectified for diffusion to yield the corresponding kinetic current values. The j_L parameter, determined combining equations (S2) and (S3), was used to make the mass transport correction. The values of j_k obtained were normalized for the total deposited mass of EC.

Tests with a rotating ring disk electrode (RRDE) were performed as well for a more complete examination of the ECs. The electrode was polished for 15 min with aluminium oxide 0.3 μm and washed with ultrapure water. The LSV experiments were conducted at 0.005 V s^{-1} and 1600 rpm in O$_2$-saturated KOH. A constant potential of 1.2 V vs RHE was applied at the Pt ring electrode. The percentage of HO$_2^-$ produced was calculated from Eq. 4 below, using the currents measured on the ring (i_R) and on the disk (i_D) electrodes, and the current collection efficiency of the ring (N).[5]

$$\% \; HO_2^- = 200 \; \times \; \frac{i_R/N}{i_D + i_R/N} \qquad \text{(S4)}$$

S1.4. Assessment of electrochemically active surface areas (ECSA)

ECSA values exhibited by electrocatalysts are usually calculated by using the following equation:

$$ECSA = C_{dl} / C_{ref} \qquad \text{(S5)}$$

where C_{dl} stands for the double-layer capacitance and C_{ref} for the reference capacitance value per unit area. Due to the impossibility of knowing the exact C_{ref} value for specific and structurally complex materials, reliable ECSA values cannot be obtained easily. However, the linear proportional relation between ECSA and the double-layer capacitance allows performing a relative comparison for similar electrocatalysts. Taking advantage of this fact, in the present work, C_{dl} values have been directly employed as approximated ECSA estimations to assess the surface effects on the ORR performances. Thus, C_{dl} values were calculated for all materials via a standard double-layer charging test, namely, the acquisition of consecutive CV plots at different scan rates (from 20 to 160 mV s^{-1}), being the double-layer capacitance estimated from the slope of a linear-fitted plot of current density at 1.13 V vs. RHE (non-faradaic region) versus the scan rate.
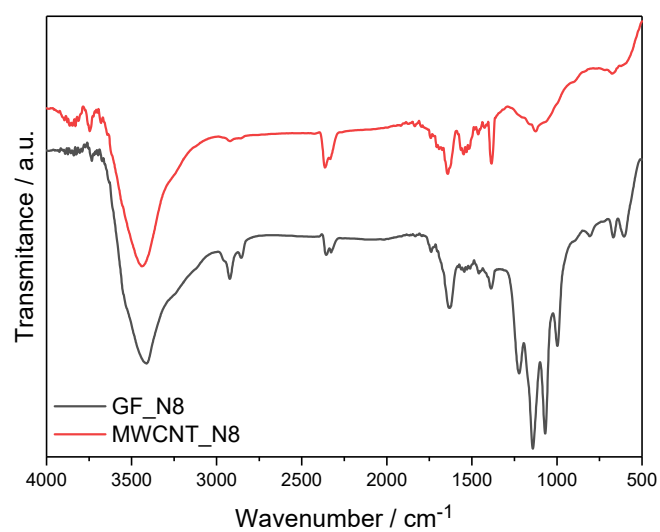
Figures

Figure S1. FTIR spectra in the 4000–500 cm^{-1} range of the nitrogen doped carbon materials GF_N8 (black) and MWCNT_N8 (red).
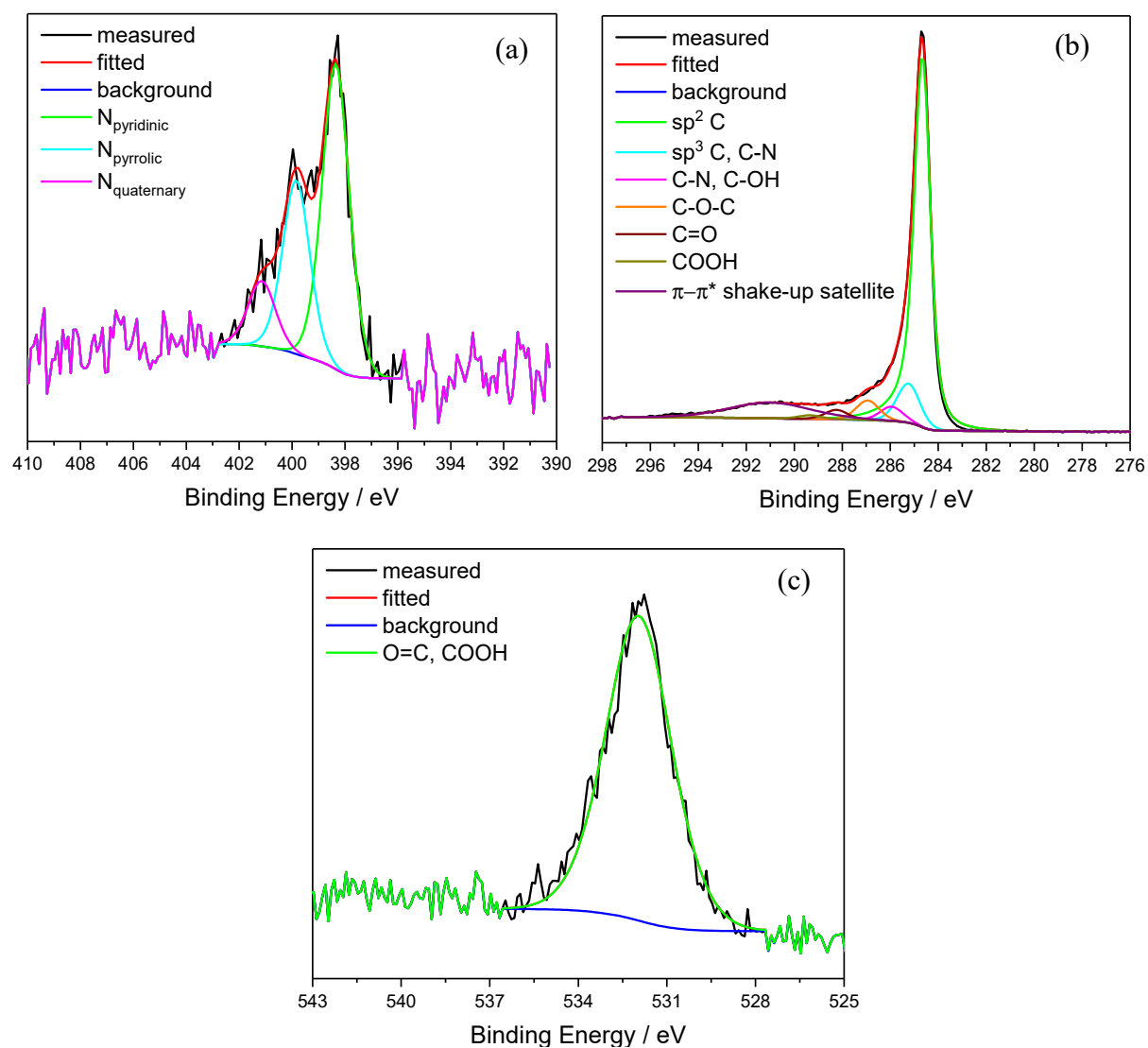
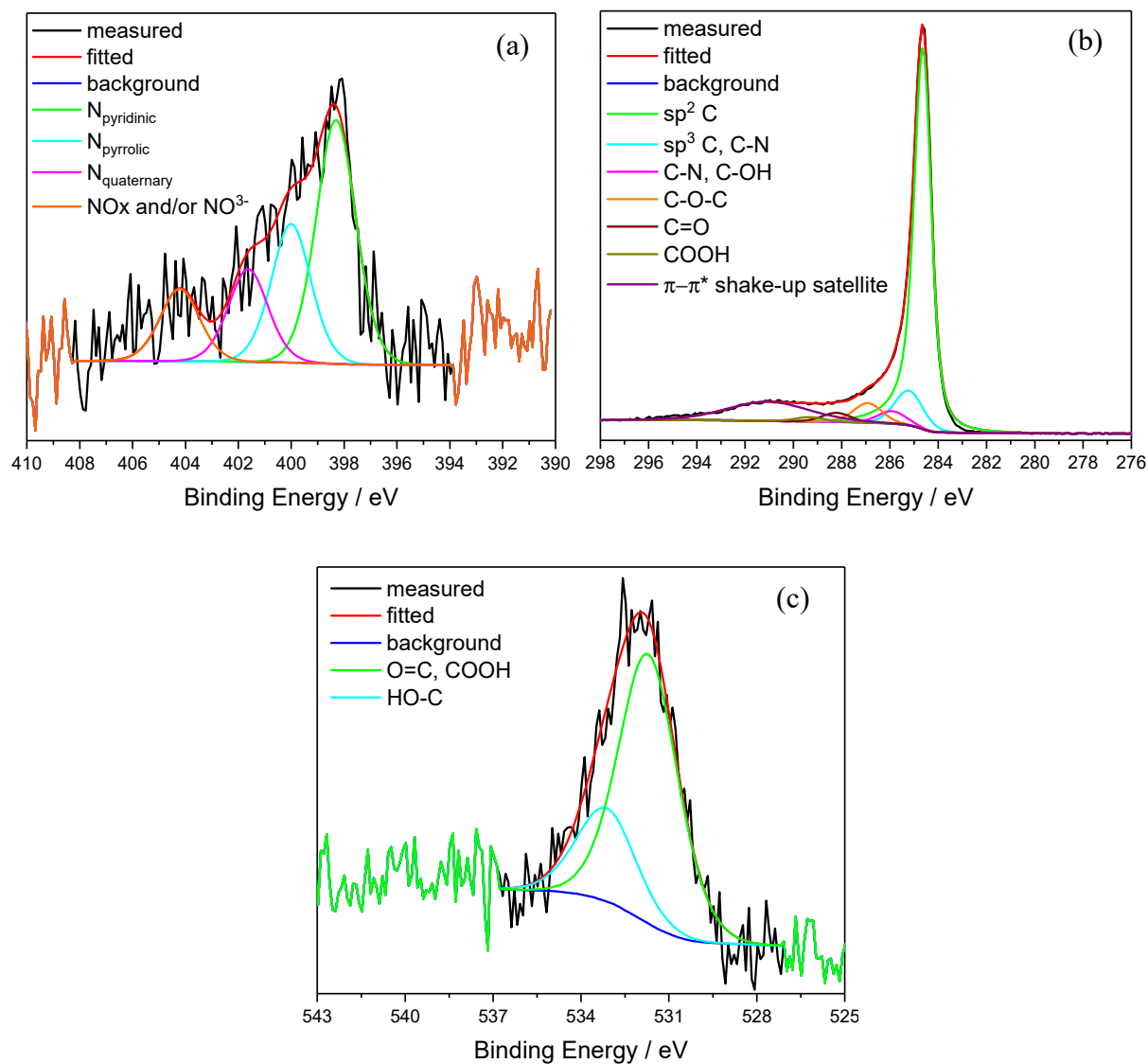**Figure S2**. XPS deconvoluted spectra of corresponding elements of the GF_N8.

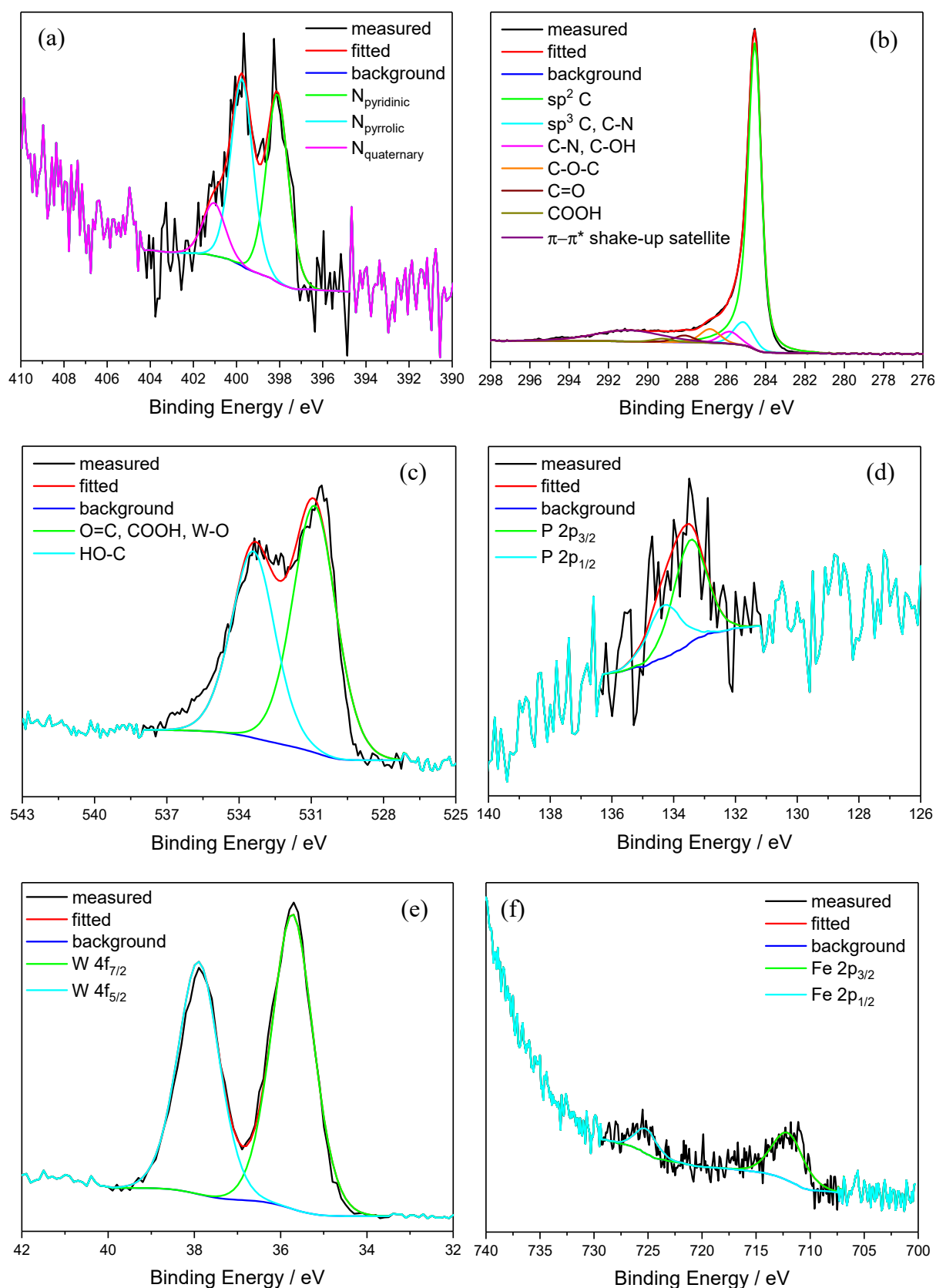**Figure S3**. XPS deconvoluted spectra of corresponding elements of the MWCNT_N8.

Figure S4. XPS deconvoluted spectra of corresponding elements in the $P_2W_{17}Fe@GF\_N8$ composite.
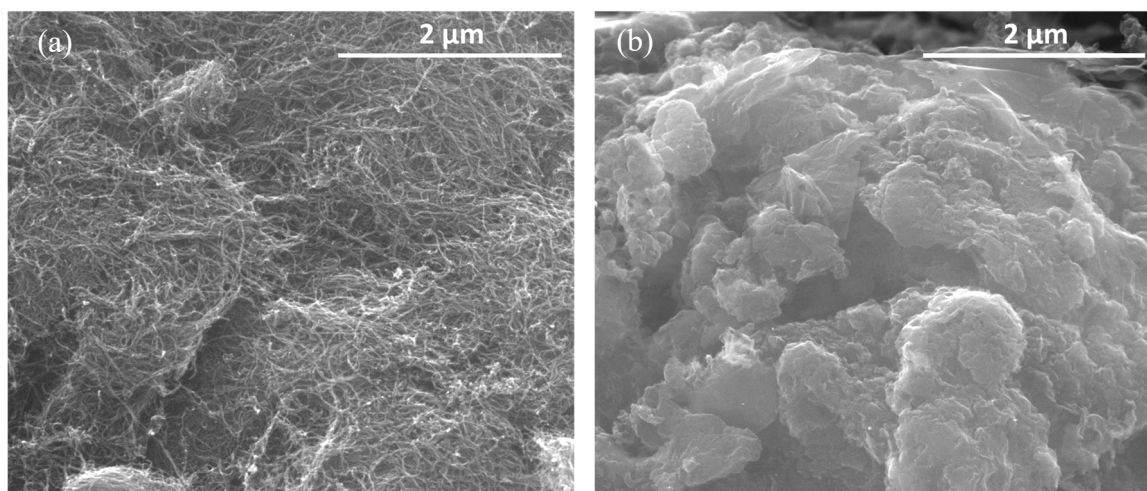
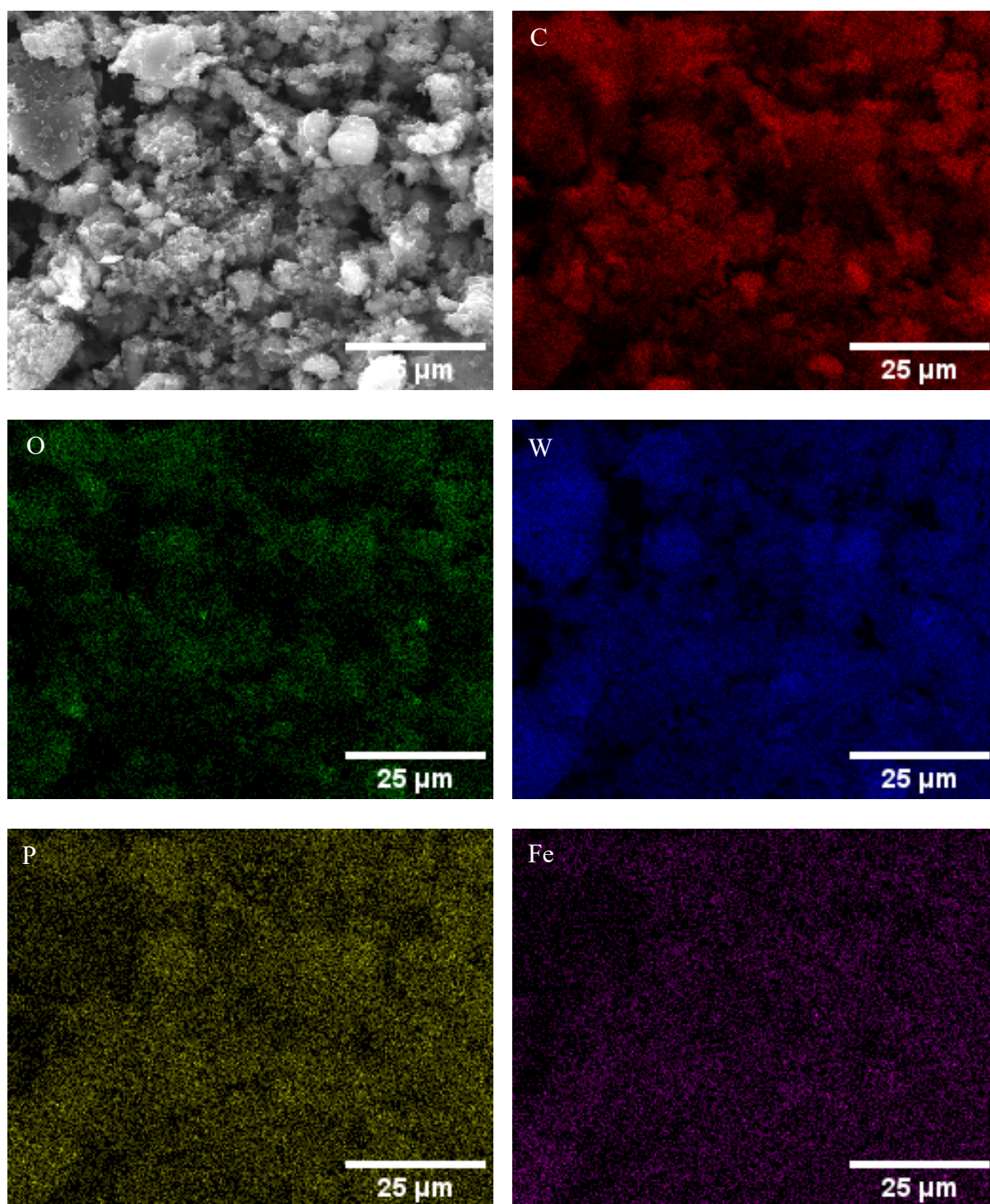**Figure S5**. SEM images of MWCNT_N8 (a) and GF_N8 (b) at 50000× magnification.

Figure S6. SEM and EDX elemental mapping images of P$_2$W$_{17}$Fe@GF_N8, at 5000×
magnification for the elements C (red), O (green), W (blue), P (yellow) and Fe (purple).
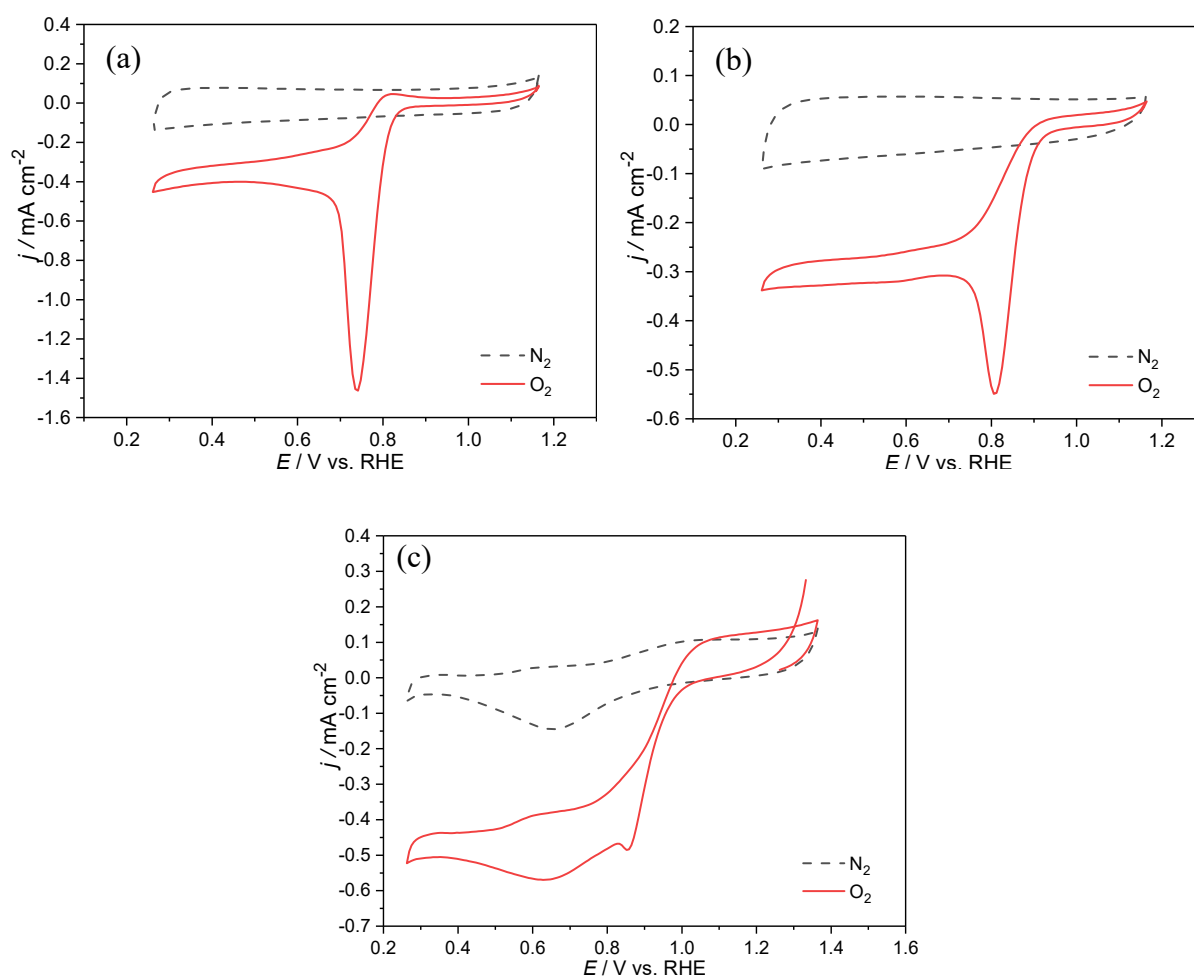
Figure S7. CVs of MWCNT_N8 (a), GF_N8 (b) and Pt/C (20 wt. %) (c) modified electrodes in N_2-saturated (dash line) and O_2-saturated (full line) 0.1 mol dm^{-3} KOH solution at 0.005 V.
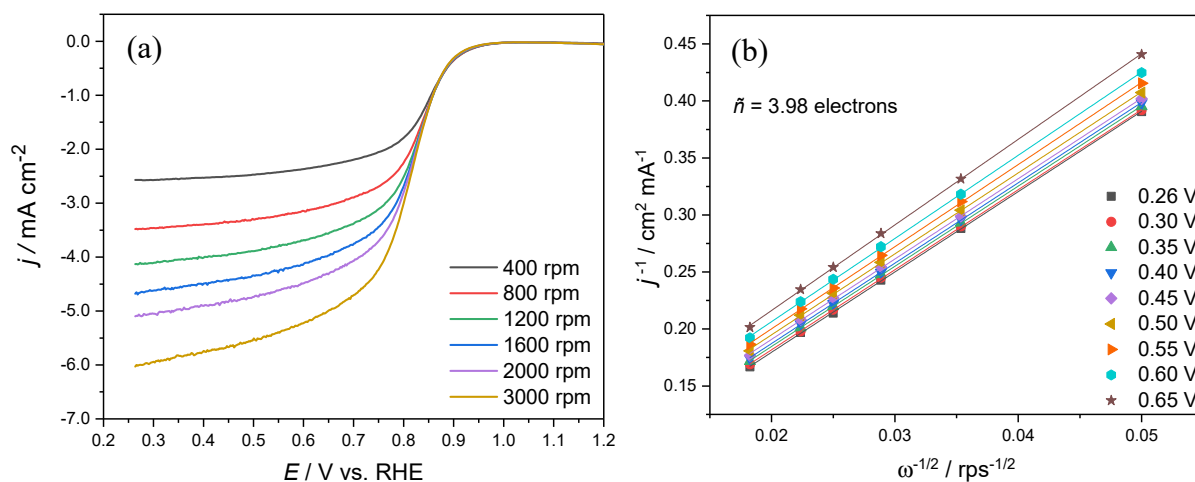
Figure S8. ORR LSV polarization curves for Pt/C (20 wt. %) at different rotation rates in O_2-saturated 0.1 mol dm^{-3} KOH solution at 0.005 V s^{-1} (a), and the corresponding Koutecky-Levich (K-L) plots (b).

Figure S9. ORR LSV polarization curves for MWCNT_N8 at different rotation rates in O_2-saturated 0.1 mol dm^{-3} KOH solution at 0.005 V s^{-1} (a), and the corresponding Koutecky-Levich (K-L) plots (b).

Figure S10. ORR polarization curves for GF_N8 at different rotation rates in O$_2$-saturated 0.1 mol dm^{-3} KOH solution at 0.005 V s^{-1} (a), and the corresponding Koutecky-Levich (K-L) plots (b).
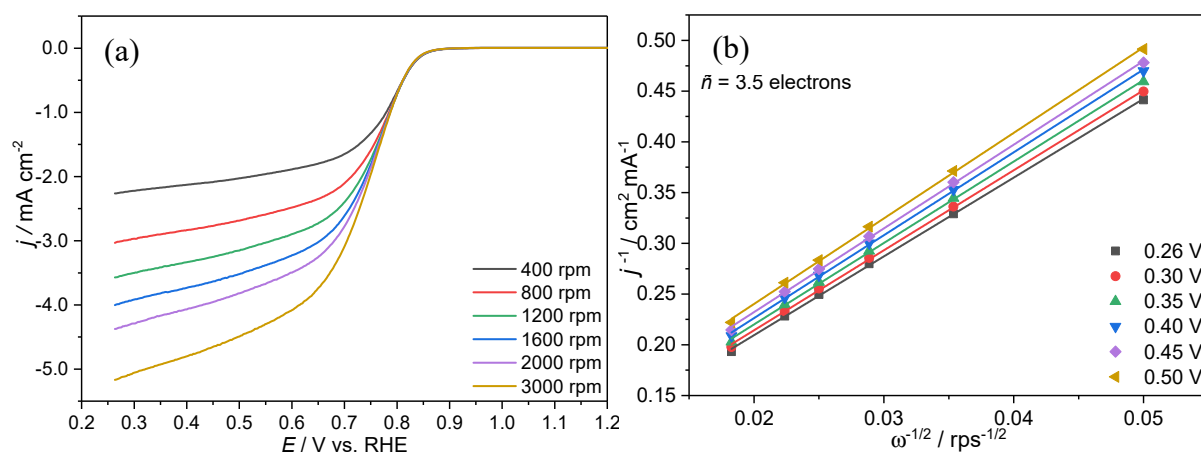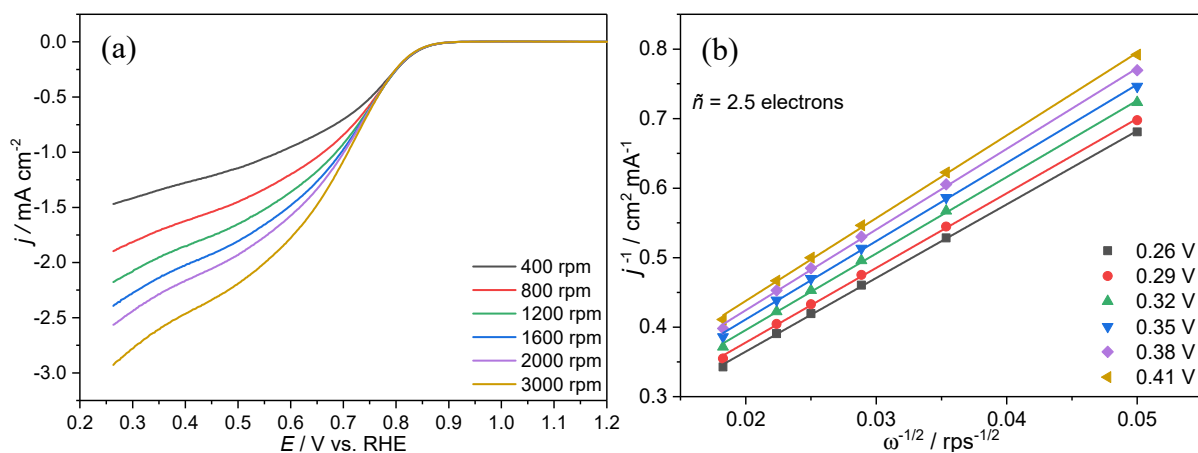

Figure S11. ORR LSV polarization curves for P$_2$W$_{17}$Fe@MWCNT_N8 at different rotation rates in O$_2$-saturated 0.1 mol dm^{-3} KOH solution at 0.005 V s^{-1} (a), and the corresponding Koutecky-Levich (K-L) plots (b).

Figure S12. ORR LSV polarization curves for $P_2W_{17}Fe@GF\_N8$ at different rotation rates in O_2-saturated 0.1 mol dm^{-3} KOH solution at 0.005 V s^{-1} (a), and the corresponding Koutecky-Levich (K-L) plots (b).
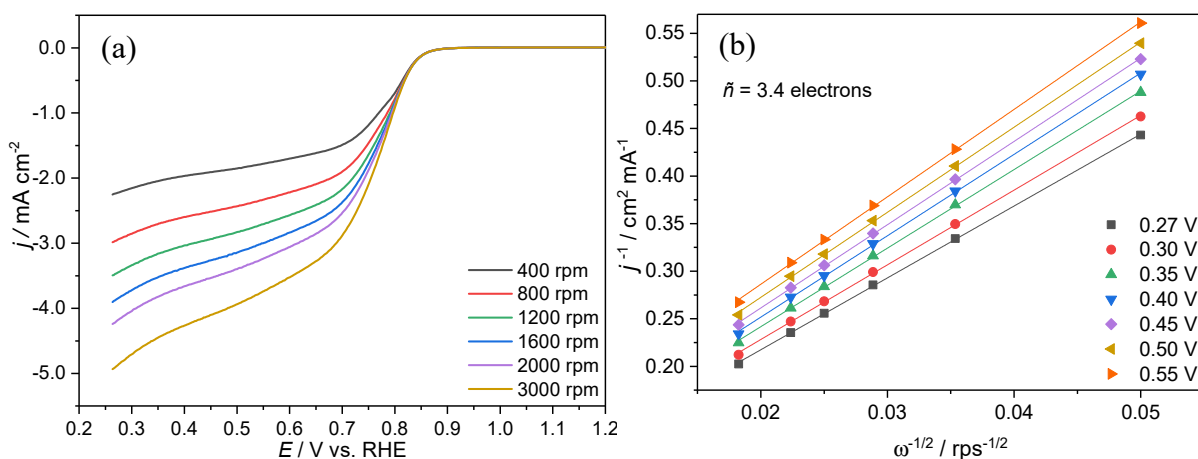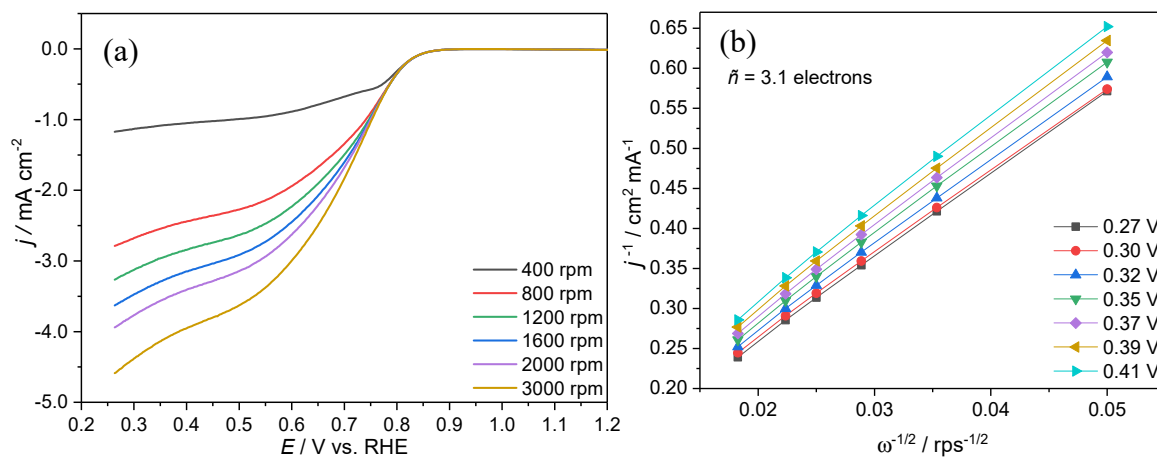
Figure S13. CVs at different scan rates for GF_N8 (a), MWCNT_N8 (b), P$_2$W$_{17}$Fe@GF_N8 (c), P$_2$W$_{17}$Fe@MWCNT_N8 (d) and Pt/C (e) in N$_2$-saturated KOH (0.1 M).
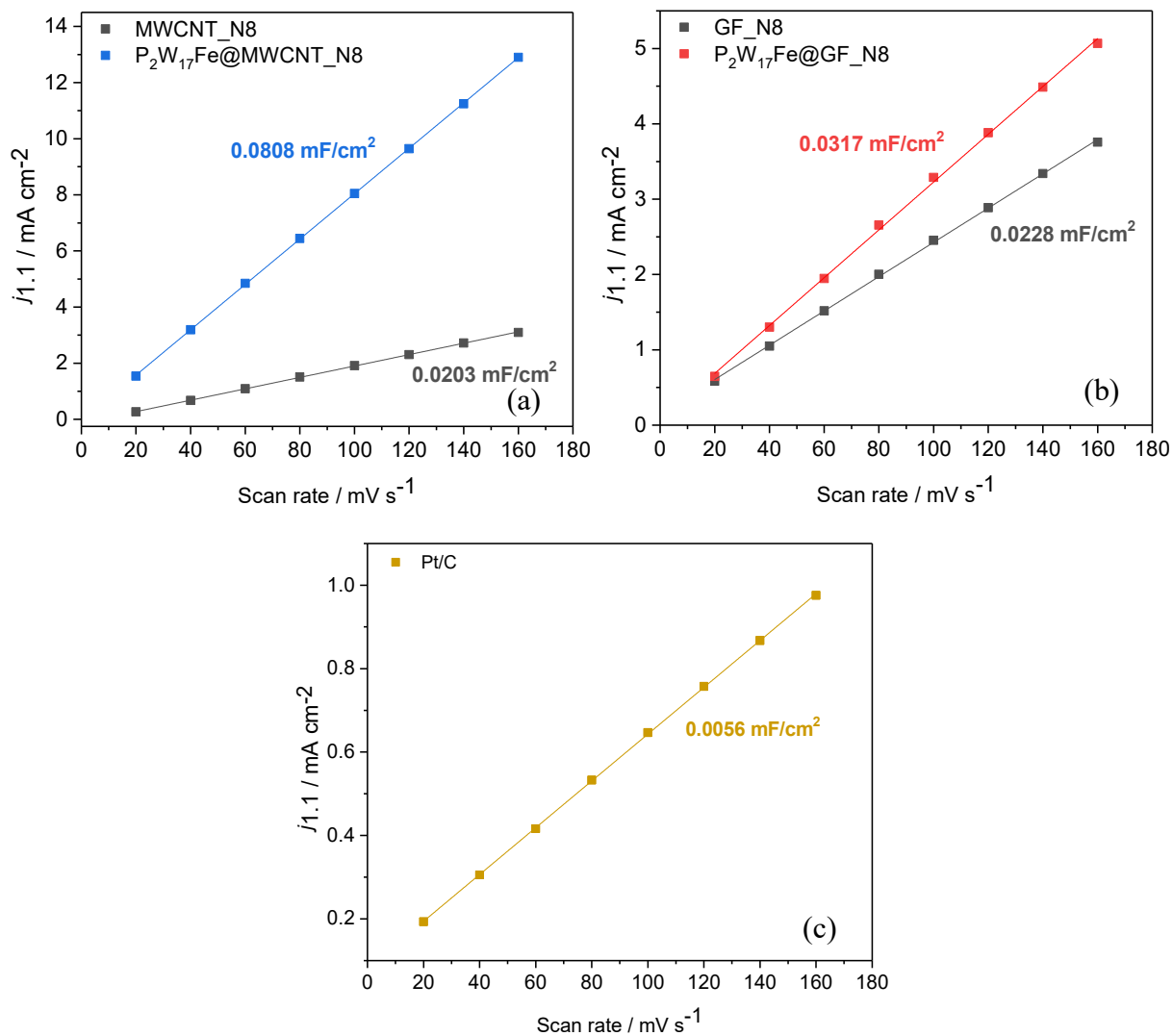
Figure S14. Current density-scan rate linear fitting plots for all materials. Numeric values correspond to the double-layer capacitances (C_{dl}) for each material.

Table S1. Relative atomic percentages of nitrogen presented in the XPS high-resolution N1s spectra of the prepared carbon materials.

Material	% N			
	398.5 eV (pyridinic N)	400.1 eV (pyrrolic N)	401.6 eV (quaternary N)	404.1 eV (N in N-oxides)
GF_N8	56.1	31.9	12.0	-
MWCNT_N8	44.6	25.3	16.9	13.2
P$_2$W$_{17}$Fe@GF_N8	44.0	43.6	12.4	-
P$_2$W$_{17}$Fe @MWCNT_N8	41.2	26.7	23.8	8.3

Table S2. ORR performance of transition metal carbon hybrid electrocatalysts obtained from literature.

Catalyst	E_{onset} (mV vs. RHE)	j_L (mA/m^2)	TS (mV/dec)	Stability[a]	Reference
P$_8$W$_{48}$@N-MWCNT	0.94	-3.7	72	82% (10h)	[6]
Co$_4$(PW$_9$)$_2$@N-CNT	0.90	-8.5	96	78% (5.5h)	[7]
N-PC[b]	0.94	-	63	81.4% (10h)	[8]
CoPOM@C	1.00	-4.2	65	-	[9]
AC$_1$[c]	0.84	-3.12	250	~80% (5.5h)	[10]
PMo$_{11}$V@GF	0.80	-1.60	177	-	[11]
MWCNT_N8_Co$_4$	0.85	-3.52	41	~75% (5.5h)	[12]
Fe$_3$O$_4$/N/C	0.92	-	-	90% (2.8h)	[13]
NiCo$_2$O$_4$/NrGO	0.88	-	-	87% (2h)	[14]
FeP/Fe$_2$P/Fe$_2$P$_2$O$_7$/C	0.86	-	-	87% (12h)	[15]
CuCo$_2$O$_4$/NrGO	0.89	-	-	85% (5.6h)	[16]
Fe-N-C	0.96	-	-	-	[17]
Fe-bNCNT/NC-900	1.02	-	57	89% (11.1h)	[18]
P$_2$W$_{17}$Fe@GF_N8	0.83	-3.3	58	68% (10h)	This work
P$_2$W$_{17}$Fe@MWCNT_N8	0.84	-3.9	48	88% (10h)	This work

[a] The percentages are of current retention and between bracket is the time; [b] N-doped porous carbon; [c] Biomass residue (Agave sisalana).

References

1. D. K. Lyon, W. K. Miller, T. Novet, P. J. Domaille, E. Evitt, D. C. Johnson and R. G. Finke, *Journal of the American Chemical Society*, 1991, **113**, 7209-7221.

2. N. Daems, X. Sheng, I. F. J. Vankelecom and P. P. Pescarmona, *Journal of Materials Chemistry A*, 2014, **2**, 4085-4110.

3. S. Hoang, S. Guo, N. T. Hahn, A. J. Bard and C. B. Mullins, *Nano Letters*, 2012, **12**, 26-32.

4. G. Tuci, C. Zafferoni, A. Rossin, A. Milella, L. Luconi, M. Innocenti, L. Truong Phuoc, C. Duong-Viet, C. Pham-Huu and G. Giambastiani, *Chemistry of Materials*, 2014, **26**, 3460-3470.

5. N. Muthuswamy, M. E. M. Buan, J. C. Walmsley and M. Rønning, *Catalysis Today*, 2018, **301**, 11-16.

6. H. C. Novais, B. Jarrais, A. Haider, U. Kortz, A. Guerrero-Ruiz, I. Rodriguez-Ramos, C. Freire and D. M. Fernandes, *Electrocatalysis*, 2023, **14**, 294-305.

7. D. M. Fernandes, H. C. Novais, R. Bacsa, P. Serp, B. n. Bachiller-Baeza, I. Rodríguez-Ramos, A. Guerrero-Ruiz and C. Freire, *Langmuir*, 2018, **34**, 6376-6387.

8. X. Chen, W. Zhang, Y. Qu, X. Chen, Y. Liu and C. Lu, *Journal of Electroanalytical Chemistry*, 2022, **926**, 116909.

9. S. Ingavale, I. Patil, K. Prabakaran and A. Swami, *International Journal of Energy Research*, 2021, **45**, 7366-7379.

10. D. M. Fernandes, A. S. Mestre, A. Martins, N. Nunes, A. P. Carvalho and C. Freire, *Catalysis Today*, 2020, **357**, 269-278.

11. M. Nunes, D. M. Fernandes, I. M. Rocha, M. F. Pereira, I. M. Mbomekalle, P. de Oliveira and C. Freire, *ChemistrySelect*, 2016, **1**, 6257-6266.

12. N. Limani, I. S. Marques, B. Jarrais, A. J. Fernandes, C. Freire and D. M. Fernandes, *Catalysts*, 2022, **12**, 357.

13. Y. Su, H. Jiang, Y. Zhu, X. Yang, J. Shen, W. Zou, J. Chen and C. Li, *Journal of Materials Chemistry A*, 2014, **2**, 7281-7287.

14. H. Zhang, H. Li, H. Wang, K. He, S. Wang, Y. Tang and J. Chen, *Journal of Power Sources*, 2015, **280**, 640-648.

15. Z. Yang, J. Wu, X. Zheng, Z. Wang and R. Yang, *Journal of Power Sources*, 2015, **277**, 161-168.

16. R. Ning, J. Tian, A. M. Asiri, A. H. Qusti, A. O. Al-Youbi and X. Sun, *Langmuir*, 2013, **29**, 13146-13151.

17. M. M. Hossen, K. Artyushkova, P. Atanassov and A. Serov, *Journal of Power Sources*, 2018, **375**, 214-221.

18. F. Lu, K. Fan, L. Cui, B. Li, Y. Yang, L. Zong and L. Wang, *Applied Catalysis B: Environmental*, 2022, **313**, 121464.